Open quantum rotors: Connecting correlations and physical currents

Ricardo Puebla [1,2,*] Alberto Imparato,[3,*] Alessio Belenchia [4,2] and Mauro Paternostro[2]

[1]*Instituto de Física Fundamental, IFF-CSIC, Calle Serrano 113b, 28006 Madrid, Spain*
[2]*Centre for Quantum Materials and Technologies, School of Mathematics and Physics,*
Queen's University, Belfast BT7 1NN, United Kingdom
[3]*Department of Physics and Astronomy, University of Aarhus, Ny Munkegade, Building*
1520, DK-8000 Aarhus C, Denmark
[4]*Institut für Theoretische Physik, Eberhard-Karls-Universität Tübingen, 72076 Tübingen, Germany*

We consider a finite one-dimensional chain of quantum rotors interacting with a set of thermal baths at different temperatures. When the interaction between the rotors is made chiral, such a system behaves as an autonomous thermal motor, converting heat currents into nonvanishing rotational ones. Such a dynamical response is strongly pronounced in the range of the Hamiltonian parameters for which the ground state of the system in the thermodynamic limit exhibits a quantum phase transition. Such working points are associated with large quantum coherence and multipartite quantum correlations within the state of the system. This suggests that the optimal operating regime of such a quantum autonomous motor is one of maximal quantumness.

I. INTRODUCTION

There is a growing, cross-disciplinary interest in the understanding of the way quantum features affect the laws of thermodynamics [1–5] and explore the limits to thermal machines operating at the nanoscale [6–12]. While, so far, the focus of such investigations has been primarily put on simple quantum systems involving only a few degrees of freedom, the assessment of the thermodynamic performance of quantum many-body systems as working media of potential quantum motors have recently started to receive attention [13–18].

Autonomous thermal motors are of particular interests for the thermodynamics of both classical [19–24] and quantum processes [25–31]. Such devices are able to convert thermal currents into motion, and thus possibly work. Their most salient feature is that they can operate without the intervention of an external agent that changes their Hamiltonian, making their design ideal for application purposes. Autonomous quantum refrigerators have a similar task, cooling down a reservoir at the expenses of heath currents [32–34].

Recent work has shown that collective phenomena such as synchronization and classical phase transitions can enhance the dynamic and thermodynamic performances in systems of interacting molecular motors [35–37], of interacting work-to-work transducers [38–40], in a 2D system of classical rotors driven out of equilibrium by a temperature gradient [41], or in an out-of-equilibrium Frenkel-Kontorova model undergoing a commensurate-incommensurate phase transition [24]. These are a fascinating phenomena arising from the collective behavior in a many-body system [42], which divide the phases of matter characterized by different properties depending on the external conditions. This phenomenon also applies to quantum systems, where quantum fluctuations—rather than thermal ones—can trigger quantum phase transitions (QPTs) [43]. At a quantum critical point, the ground state of the system develops singular behavior, typically accompanied by the closing of the energy gap [43] with the first excited state and diverging quantum correlations [44–46], among other features.

The study of autonomous thermal motors and refrigerators based on quantum many-body effects could thus potentially allow for the identification of possible performance enhancements stemming from collective quantum phenomena such as a QPT. In this paper, we investigate the thermodynamics of an autonomous system in proximity of a QPT. We consider a finite-size one-dimensional chiral clock model (CCM) consisting of interacting quantum rotors. In the thermodynamic limit of infinitely many constituents, this model exhibits a well-characterized QPT [47–50]. A dimer of quantum rotors with chiral interaction has been shown to give rise to a rotational current, when connected to two baths at different temperatures, as a result of the lack of thermal equilibrium and owing to the broken rotational symmetry [30]. In the multicomponent system considered here, we find that such a dynamical response is maximal for values of the Hamiltonian parameters that result in a QPT in the thermodynamic limit. Although the rotational current turns out to always be finite, such a phenomenon is reminiscent of the diverging response to a change in an external thermodynamic force in systems at equilibrium in proximity of a phase transition, a phenomenon whose onset we are able to witness despite the finiteness of the system that we address. Furthermore we elucidate the relation between quantum correlations and

---

thermodynamic currents in the considered CCM. While the unveiled phenomenology does not imply necessarily a causal link between the emergence of mechanical currents and the onset of many-body criticality, the interplay between these effects is suggestive of a strong role played by collective phenomena on the performance of heat-to-mechanical current conversion in such autonomous device. We emphasize that in this paper we only study the rotational currents of the rotors and the heat currents exchanged with the baths. The problem of work extraction entails the conversion of rotational motion into linear motion, a problem of technological interest, but of difficult implementation in the microscopic realm.

The remainder of this paper is organized as follows. In Sec. II, we introduce the basics of the CCM. In Sec. III, we consider the interaction of the rotors with independent thermal baths with staggered temperatures. We characterize the nonequilibrium steady state (NESS) of the model by looking at the tunneling and thermal currents. In Sec. IV, we connect the particle currents at the steady state with the correlations established within the clock model. Finally, in Sec. V, we summarize the main findings reported in the article.

II. CHIRAL CLOCK MODEL: QUANTUM PHASE TRANSITION IN THE ISOLATED SYSTEM

Let us start by considering the $\mathbb{Z}_{N_s}$ CCM for M quantum rotors [30,47–52], i.e., M quantum systems with N_s discrete energy levels. Each individual rotor can be seen as a spin-$(N_s - 1)/2$ or as particles occupying the N_s vertexes of a regular polygon. We call $\{|j_k\rangle\}$ the orthogonal basis of the Hilbert space of the kth rotor, with $j_k = 0, \ldots, N_s - 1$ denoting the N_s directions along which the angular momentum can point (or vertices of the polygon) and $|j_k + N_s\rangle = |j_k\rangle$. The CCM is then described by the Hamiltonian

$$H_{\text{ccm}} = -f \sum_{k=1}^{M} (\sigma_k + \sigma_k^\dagger) - (1 - f) \sum_{k=1}^{M} (\mu_k \mu_{k+1}^\dagger e^{i\varphi_k} + \text{H.c.}),$$

(1)

where f is the control parameter that accounts for the relative weight between the free and interaction terms, and φ_k the so-called chiral phases. We assume periodic boundary conditions, so that $\mu_{M+1} = \mu_1$. Here the local operators μ_k and σ_k for the kth rotor, are defined, in the vertex basis introduced above, as

$$\mu_k = \begin{bmatrix} 1 & 0 & 0 & \cdots & & 0 \\ 0 & \upsilon & 0 & \cdots & & 0 \\ 0 & 0 & \upsilon^2 & \cdots & & 0 \\ 0 & 0 & 0 & \ddots & & 0 \\ 0 & 0 & 0 & 0 & & \upsilon^{N_s-1} \end{bmatrix},$$

$$\sigma_k = \begin{bmatrix} 0 & 1 & 0 & 0 & \cdots & 0 \\ 0 & 0 & 1 & 0 & \cdots & 0 \\ 0 & 0 & 0 & 1 & \cdots & 0 \\ 0 & 0 & 0 & 0 & \ddots & 0 \\ 0 & 0 & 0 & 0 & \cdots & 1 \\ 1 & 0 & 0 & 0 & \cdots & 0 \end{bmatrix}$$

(2)
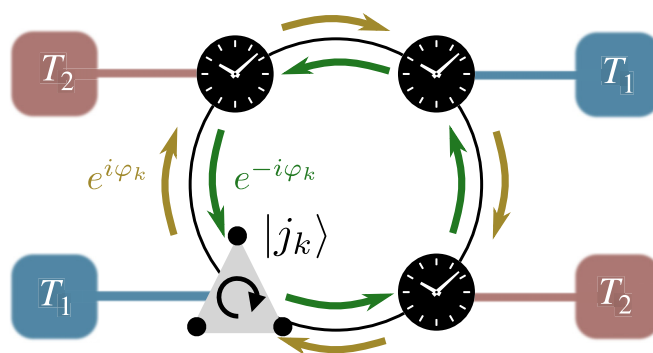
FIG. 1. Schematic representation of the CCM with periodic boundary conditions, interacting with thermal reservoirs with staggered temperatures T_1 and T_2, and chiral nearest-neighbor interactions with phases φ_k. In this illustration one of the individual rotors, or clocks, is depicted by a polygon whose vertices correspond to its internal levels $|j_k\rangle$ (for $N_s = 3$), which are coupled with an interaction strength f [cf. Eq. (1)]. In the classical picture, a mechanical (or rotational) current corresponds to the steady state directed rotation of a particle hopping between the N_s vertices of the polygon.

with $\upsilon = e^{i2\pi/N_s}$. The first term of the Hamiltonian encodes the dynamics of the individual rotors and gives rise to tunneling currents between their internal levels (cf. Fig. 1). For a particle at the vertices of a regular polygon, the tunneling currents can be visualised as describing the hopping of the single system between such vertices induced by the rotor internal Hamiltonian. The second term in the Hamiltonian encodes the interaction between nearest neighbors.

The model possesses a global $\mathbb{Z}_{N_s}$ symmetry and, classically, presents two phase transitions in 2D [53]. The interaction potential breaks a specific rotational symmetry when $\varphi_k \neq q\pi/N_s$ ($q \in \mathbb{Z}$) in a dimer ($M = 2$) Refs. [30], while on a lattice model with periodic boundary conditions the same broken symmetry arises when a staggered phase is considered [41]. This is a necessary condition for the emergence of the rotational (particle) currents, as we will also see in the following (cf. Sec. III A). In this context, the order parameter of the model is the total magnetization $m = \sum_k (\mu_k + \mu_k^\dagger)/M$. From now on, we will focus on the minimal configuration allowing for nonzero currents, namely the case of $N_s = 3$. It should be noted that, our model is similar to the one investigated in Ref. [50] where the role of σ and μ was interchanged. There, it was argued that the phase transition experimentally found in a one–dimensional chain of trapped alkali-metal atoms [54] belongs to the universality class of the $\mathbb{Z}_3$ chiral clock model considered here. In Refs. [49,50], the structure of the phase diagram of the CCM with $N_s = 3$ and homogeneous chiral phase $\varphi_k = \varphi$ was investigated in detail, showing that for small values of φ there is a direct transition from the ordered ($f \ll 1/2$) to a disordered phase ($f \gg 1/2$). For large chirality ($\varphi > \pi/6$), the two phases are separated by an incommensurate phase. In Appendix A, we provide a brief summary of the symmetry-breaking QPT taking place in the ground state of H_{ccm}, while we refer to Refs. [49,50] for a thorough inspection of the model's critical features.

III. OPEN SYSTEM DYNAMICS: CORRELATIONS VS CURRENTS

We are interested in exploring the physics of the CCM when interacting with thermal baths. In particular, we consider the case in which each rotor is in contact with an independent thermal reservoir and partition our system in two sub-lattices consisting of even (e) and odd (o) rotors, respectively. The inverse temperature of the two sub-lattices is set to be β_e and β_o, respectively, and we will assume $\beta_e \neq \beta_o$, in general, thus realizing a staggered-temperature configuration (cf. Fig. 1 for a schematic illustration). As it will be shown later on in this section, the temperature difference gives rise to thermally driven mechanical currents in the system that are sustained asymptotically in time. The system thus evolves towards a nonequilibrium steady state (NESS), whose properties we now aim at characterizing.

We describe the open system dynamics via the local Gorini-Kossakowski-Sudarshan-Lindblad (GKLS) master equation

$$\dot{\rho} = -i[H_{\mathrm{ccm}}, \rho] + \sum_{k=1}^{M} \mathcal{D}_k(\rho), \tag{3}$$

with local dissipators

$$\mathcal{D}_k[\bullet] = \sum_{j,j'} W_{j,j'}^{(k)} \left[L_{j,j'}^{(k)} \bullet L_{j,j'}^{(k),\dagger} - \frac{1}{2} \left\{ L_{j,j'}^{(k),\dagger} L_{j,j'}^{(k)}, \bullet \right\} \right]. \tag{4}$$

defined in terms of the jump operators $L_{j,j'}^{(k)} = |j\rangle\langle j'|$ with $|j\rangle = |j_1, \ldots, j_M\rangle$ with $j_k = 0, \cdots, N_s - 1$. Each of the local dissipators $L_{j,j'}^{(k)}$ induces an incoherent transition between states $|j\rangle$ and $|j'\rangle$, weighted by the rate $W_{j,j'}^{(k)}$, where only the spin of the kth rotor is rotated, that is, $|j\rangle \equiv |j_1, \ldots, j_k, \ldots, j_M\rangle \to |j'\rangle \equiv |j_1, \ldots, j_k \pm 1, \ldots, j_M\rangle$.

The transition rates $W_{j,j'}$ from $|j'\rangle$ to $|j\rangle$ fulfill the local detailed balance

$$W_{j,j'}^{(k)} / W_{j',j}^{(k)} = e^{\beta_k(E_{j'} - E_j)}, \tag{5}$$

where $E_j = \langle j | H_{\mathrm{ccm}} | j \rangle$. The energies E_j entering the local detailed balance condition Eq. (5) are not eigenvalues of the total system Hamiltonian H_{ccm} as a consequence of the choice of local basis $\{|j_k\rangle\}$ defining the jump operators, see, for instance, Refs. [46,55]. For the transition rates, we take $W_{j,j'}^{(k)} = \gamma_k(E_{j'} - E_j)$ with

$$\gamma_k(\omega) = \frac{g|\omega|}{1 - e^{-\beta_k|\omega|}} \zeta(\omega) \quad \text{and} \quad \zeta(\omega) = \begin{cases} e^{\beta_k \omega} & \omega \leqslant 0, \\ 1 & \omega > 0, \end{cases} \tag{6}$$

so as to match the corresponding expression for a generic bosonic bath with global detailed balance [56], and where g is a microscopic rate. Before proceeding further, a note is in order. As it is well known, local master equations can be problematic from a thermodynamic point of view [57,58]. However, it should be noted that this conclusion has been recently challenged by a stream of works [34,59–61] pointing towards a reconciliation of local master equation and thermodynamics. In particular, it has been shown that the local master equation is not, in general, at odds with the second law of thermodynamics as far as the proper expression for the heat

currents is considered. In the specific case under study, we can split the Hamiltonian in its diagonal and nondiagonal part in the $\{|j\rangle\}$ basis as $H_{\mathrm{ccm}} = H_D + H_{ND}$, which allows us to introduce the individual energy currents

$$\dot{Q}_{D,k} = \mathrm{tr}(\rho \mathcal{D}_k^*[H_D]), \quad \dot{Q}_{ND,k} = \mathrm{tr}(\rho \mathcal{D}_k^*[H_{ND}]), \tag{7}$$

where $\mathcal{D}_k^*$ is the dual of $\mathcal{D}_k$. In the steady state $\dot{\rho} = 0$, and using the adjoint master equation of (3), one obtains the energy conservation condition, that reads

$$d_t \langle H_{\mathrm{ccm}} \rangle = 0 = \sum_k \dot{Q}_{D,k} + \dot{Q}_{ND,k}. \tag{8}$$

It is useful to remark that the *standard* definition of heat flux when dealing with a local master equation would read $\dot{Q}_k = \mathrm{tr}(\rho \mathcal{D}_k^*[H_{\mathrm{ccm}}]) = \dot{Q}_{D,k} + \dot{Q}_{ND,k}$. Unfortunately, using $\dot{Q}_k$ leads in general to violations of the second law of thermodynamics (cf. Ref. [57] for an example). However, it is the weighted sum of $\dot{Q}_{D,k}$'s that enters the second law of thermodynamics and gives a positive entropy production rate $\dot{\Sigma} = dS/dt - \sum_k \beta_k \dot{Q}_{D,k} \geqslant 0$, consistently with the second law [34], and one should really focus on the individual currents. Equation (3) can be derived starting from a microscopic model for the baths, the system, and the interaction Hamiltonian. At such microscopic level, energy conservation holds for the total Hamiltonian (baths, system, bath–system interaction). Eq. (8) expresses energy conservation for the system alone, when its dynamic has already been coarse-grained. Thus by interpreting the first term on the right-hand side of such equation as the heat current flowing into the system from the baths [34], we can conclude that the nondiagonal term is the residue energy flowing into/from the system because of the mismatch between the eigenbasis of the Hamiltonian and the chosen system-bath interaction described by the jump operators $L_{j,j'}$. Furthermore, in another consistent thermodynamic interpretation $\dot{Q}_{ND,k}$ can be associated to a work rate within a microscopic collisional model framework [61]. For further details on this construction, we refer the interested reader to Ref. [34]. An alternative approach to the thermodynamic consistency of the local master equations is discussed, e.g., in Ref. [62].

A. NESS of the GKLS master equation and particle currents

From the numerical diagonalization of the Liouville superoperator on the right-hand-side of the GKLS master equation, we obtain the unique steady state ρ_{SS} of the CCM interacting with independent thermal baths. Such state is in general a NESS, however its nature is determined by the choice of parameters of the model. Note that, although the ground state of H_{ccm} displays a QPT, such abrupt transition is blurred in this open quantum system setting. In order to quantify the nonequilibrium nature of the steady state we turn to look at quantum particle currents in the system.

The definition of quantum particle currents in general is a non trivial task. A formal characterisation has been carried out in Ref. [30] where the authors also investigate a CCM with $M = 2$ rotors. For a classical particle hopping on a graph, one can readily define the probability current between any two vertices on the graph which reads

$$J_{j \to j'} = W_{j'j} p_j - W_{jj'} p_{j'}, \tag{9}$$

where p_j is the instantaneous probability of finding the particle at vertex j, and $W_{jj'}$ is the transition rate from j' to j. In Ref. [30], the quantum analog of this classical current was defined as the sum of the tunneling and thermal current operators, namely,

$$J_{j \to j'}^{\text{tun}} = i(x_j H_{\text{ccm}} x_{j'} - x_{j'} H_{\text{ccm}} x_j), \qquad (10)$$

$$J_{j \to j'}^{\text{th}} = \frac{1}{2} \sum_{k, \mathsf{j}, \mathsf{j}'} W_{\mathsf{j}, \mathsf{j}'}^{(k)} \big[\{ x_j, L_{\mathsf{j}, \mathsf{j}'}^{(k),\dagger} x_{j'} L_{\mathsf{j}, \mathsf{j}'}^{(k)} \} - \{ x_j', L_{\mathsf{j}, \mathsf{j}'}^{(k),\dagger} x_j L_{\mathsf{j}, \mathsf{j}'}^{(k)} \} \big],$$
$$(11)$$

where $x_j = |j\rangle\langle j|$ is the projector onto a generic state $|j\rangle$, $L_{\mathsf{j}, \mathsf{j}'}^{(k)} = |\mathsf{j}\rangle\langle \mathsf{j}'|$ is the jump operator for the kth rotor between states $|\mathsf{j}\rangle$ and $|\mathsf{j}'\rangle$ which is weighted by the thermal rate of the kth bath, and the sum runs over all the possible transitions between pair of states of the system and over all the baths. Note that in Eq. (11), we have introduced the summation indices j and j' in order to distinguish them from the indices j and j' denoting the initial and final states of the transition under consideration. Note that the thermal current reduces to the classical probability current (9) in the classical limit. Recall that we consider jump operators $L_{\mathsf{j}, \mathsf{j}'}^{(k)}$ where only the spin of the kth rotor is rotated, namely, $L_{\mathsf{j}, \mathsf{j}'}^{(k)} = |j\rangle\langle j'|$ with $|j\rangle \equiv |j_1, \ldots j_k \ldots, j_M\rangle \to |j'\rangle \equiv |j_1, \ldots j_k \pm 1 \ldots, j_M\rangle$. We will thus refer to the overall rotational (or mechanical) current of the kth rotor as given by the sum of the two contributions stemming from Eqs. (10) and (11).

Before proceeding further, we shall discuss the general properties of these NESS currents. In order to simplify the notation, in the following, we will omit the subscript $j \to j'$ in the steady state currents $\langle J_{j \to j'}^{\text{tun,th}} \rangle$, as in the NESS the rotational currents of the kth rotor are independent of the specific initial and final position considered. We consider staggered chiral phases $\varphi_k = (-1)^k \varphi$, which, as discussed below, give homogeneous currents within each of the two sublattices. For $\varphi = q\pi/N_s$ ($q \in \mathbb{Z}$), the currents vanish, $\langle J^{\text{tun}} \rangle_k = \langle J^{\text{th}} \rangle_k = 0$, for each individual rotor $k = 1, \ldots, M$, $\forall f$ and regardless of the temperature difference among sub-lattices $\Delta T = 1/\beta_o - 1/\beta_e$. The choice $\varphi_k = (-1)^k \varphi$ makes the system rotationally asymmetric, which is a prerequisite for directed rotational currents to arise [41]. Symmetry is restored when $\varphi = q\pi/N_s$, and thus the currents vanish. While other symmetry-breaking choices for the chiral phases are possible, the staggered setup makes the properties within each of the two sublattices homogeneous.

In addition, $\langle J^{\text{tun}} \rangle_k \neq 0$ if $\varphi \neq q\pi/N_s$ and $f \neq 0, 1$, and $\langle J^{\text{tun}} \rangle_T = \sum_{k=1}^M \langle J^{\text{tun}} \rangle_k = 0$ when $\Delta T = 0$. In a similar fashion, the thermal current fulfills $\langle J^{\text{th}} \rangle_T = \sum_k \langle J^{\text{th}} \rangle_k \neq 0$ for $\varphi \neq q\pi/N_s$ and $f \neq 1$, while $\langle J^{\text{th}} \rangle_T = 0$ for $\Delta T = 0$. Thus a nonvanishing temperature gradient $\Delta T \neq 0$ is necessary for a net motor effect with nonvanishing $\langle J^{\text{tun}} \rangle_T$ and $\langle J^{\text{th}} \rangle_T$ to arise. Figure 2 shows the individual steady state currents as a function of f and φ for each of the individual rotors (at even or odd sites) in a CCM with $M = 6, N_s = 3, \beta_e = 1, \beta_o = 1.1$, and $g = 0.2$, which already reveal a nontrivial behavior. The choice of staggered temperatures and chiral phases gives equal currents within each sublattice. A similar behavior is found for different parameter combinations. Inspection of Fig. 2
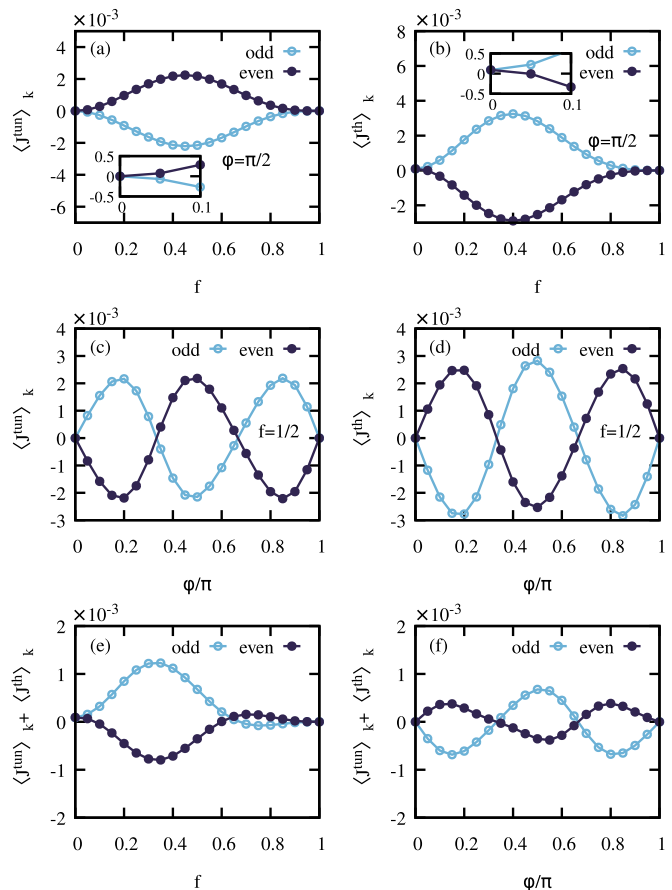
FIG. 2. Behavior of the NESS tunneling and thermal currents $\langle J_{0 \to 1}^{\text{tun}} \rangle_k$ and $\langle J_{0 \to 1}^{\text{th}} \rangle_k$ for each rotor (at even or odd site) in a chain with $M = 6$ and $N_s = 3$. (a) and (b) [(c) and (d)] illustrate such currents as functions of f [φ with $\varphi_k = (-1)^k \varphi$] for $\beta_e = 1$ and $\beta_o = 1.1$ with $g = 0.2$. (a) and (b) have been obtained taking fixed staggered chiral phases $\varphi_k = (-1)^k \pi/2$. The insets show the behavior of currents in the region close to $f = 0$. Note that $\langle J_{0 \to 1}^{\text{tun}} \rangle = 0$, while $\langle J_{0 \to 1}^{\text{th}} \rangle \neq 0$ for $f = 0$. (c) and (d) are for $f = 1/2$, and $\varphi_k = (-1)^k \varphi$. Here, the currents display a $2\pi/N_s$ periodicity in φ. (e) and (f) show the net current for each of the rotors (even or odd) as a function of f and φ, respectively. We refer to the body of the paper for further details, and to Fig. 3 for the behavior of the total currents.

suggests that the maximum of $|\langle J^{\text{tun}} \rangle_k|$ is reached at $f \approx 0.45$, which is very close to the value $f \approx 0.46$ at which a QPT occurs in the ground state of the CCM at thermodynamic limit [cf. Appendix A]. However, the thermal current $\langle J^{\text{th}} \rangle_k$ is maximized for a slightly smaller value of f. Also, the insets in Figs. 2(a) and 2(b) show that, in the *classical* limit $f = 0$, the tunneling current is vanishing in both sublattices, while the rotors exhibit the same nonzero thermal rotational frequency. Note that, in spite of the opposite sign of thermal and tunneling currents for each rotor, the net current is nonzero in general, as shown in Fig. 2(e) and (f), which show $\langle J^{\text{tun}} \rangle_k + \langle J^{\text{th}} \rangle_k$ against f and ϕ, respectively. Although not explicitly shown, the mean square value of the thermal current has a maximum at $f \approx 1/2$ while the analogous quantity for the tunneling current gets the value of $\approx 2f^2/3$ independently of φ. This value suggests that all clock states are equally
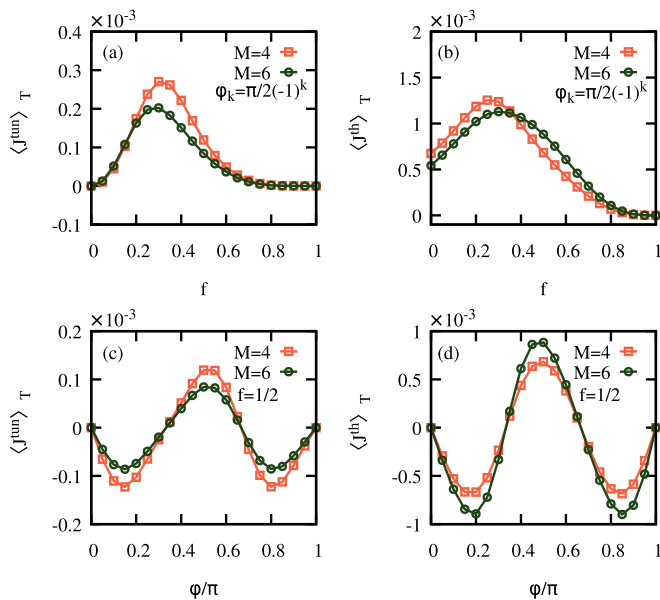
FIG. 3. Total NESS currents $\langle J^{\mathrm{tun}}\rangle_T$ and $\langle J^{\mathrm{th}}\rangle_T$ for $M = 4$ and $M = 6$ rotors and $\beta_e = 1$, $\beta_o = 1.1$ with $g = 0.2$. (a) and (b) are for $\varphi_k = (-1)^k \pi/2$, while (c) and (d) are for $f = 1/2$.

populated at the NESS.[1] However, as shown in Sec. IV, such state is not a maximally mixed one as it brings about coherence and nontrivial correlations among the individual rotors.

Figure 3 illustrates the total currents $\langle J^{\mathrm{tun,th}}\rangle_T$ for the same parameters as Fig. 2 for $M = 4$ and 6 rotors and $\Delta T \neq 0$. Note that for fixed M the total thermal current is larger than the tunneling one. Furthermore, for the two sizes here considered, $\langle J^{\mathrm{th}}\rangle_T$ is almost constant for increasing number of rotors, while $\langle J^{\mathrm{tun}}\rangle_T$ decreases its value suggesting that for large M the total tunneling current will be negligible with respect to the thermal one. Hence, in the thermodynamic limit, one should expect $\langle J^{\mathrm{th}}\rangle_T + \langle J^{\mathrm{tun}}\rangle_T \approx \langle J^{\mathrm{th}}\rangle_T$.

We now turn our attention to the steady state heat currents, as given by Eqs. (7). Here the heat currents are positive when flowing from the bath(s) to the system. The results, for two different sets of system parameters, are shown in Fig. 4. As previously done, we have chosen the even sublattice to be in contact with the hot bath. We observe that, for a small temperature gradient, the diagonal heat currents are both negative. This can be understood as follows. First, the first law—written in the form $\sum_k (\dot{Q}_{D,k} + \dot{Q}_{ND,k}) = 0$—is valid. Second, we recall that the nondiagonal heat current $\dot{Q}_{ND}$ corresponds, within the framework of the collisional model, to the work done or produced when switching on and off the interaction of the system with the colliding particles making up the environment [34,61]. Thus the situation in Fig. 4 where $\dot{Q}_{D,k} < 0$ for all rotors is compensated by a large and positive $\sum_k \dot{Q}_{ND,k}$, corresponding to a net amount of work done on the

---

[1]This can be seen from the tunneling current for the first rotor, $J^{\mathrm{tun}}_{0\to1} = if[|1\rangle\langle0| - |1\rangle\langle0|] \otimes I_{2,...,M}$. Hence, $(J^{\mathrm{tun}}_{0\to1})^2 = f^2[|0\rangle\langle0| + |1\rangle\langle1|] \otimes I_{2,...,M}$, so that $\langle(J^{\mathrm{tun}}_{0\to1})^2\rangle = \mathrm{Tr}[(J^{\mathrm{tun}}_{0\to1})^2\rho] = f^2(\mathrm{Tr}[\rho] - \sum_{j=2}^{N_s}\langle j|\rho|j\rangle)$ with ρ the NESS. If ρ populates equally each of the N_s states, then $\langle(J^{\mathrm{tun}}_{0\to1})^2\rangle = 2f^2/N_s$.
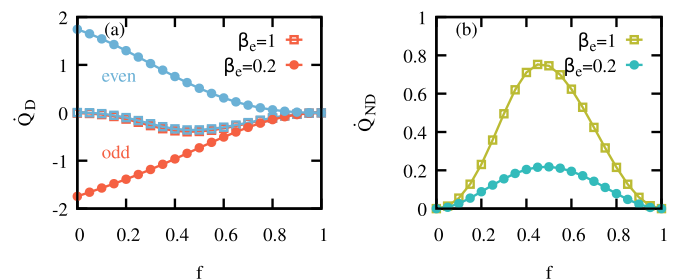
FIG. 4. Diagonal (a) and nondiagonal (b) heat currents, $\dot{Q}_{D,m}$ and $\dot{Q}_{ND} = \sum_k \dot{Q}_{ND,k}$, as defined by Eq. (7), respectively, as a function of f for the NESS of the CCM with $M = 4$ rotors and staggered chiral phases $\varphi_k = (-1)^k \pi/2$ and temperatures. We have taken $\beta_o = 1.1$, $g = 0.2$, and $\beta_e = 0.2$ and 1, as specified in the legend of the figure. In (a), we show the heat currents for each sub-lattice, namely, even and odd rotors. For $\beta_e = 1$, $\dot{Q}_D < 0$ for both sub-lattices, which implies a large nondiagonal heat current. Note that $\sum_k (\dot{Q}_{D,k} + \dot{Q}_{ND,k}) = 0$.

system that is then dissipated in both the cold and hot baths. One can understand this result also noticing that, when $f > 0$ the Hamiltonian in Eq. (1) is not diagonal in the basis $|j\rangle$. Thus Eq. (3) will introduce coherence in the steady state, resulting in a nonzero nondiagonal heat current, as given by the second line of Eq. (7).

For a larger temperature gradient, and one of the two temperatures relatively high, the heath currents exhibits a more classical behavior with a net diagonal current from the hot to the cold baths and a reduced nondiagonal heat current.

In the ground state of the system (1), the thermally driven current $\langle J^{\mathrm{th}}\rangle_k$ vanishes for any f: at $T = 0$, there is no heat current to sustain the rotational motion. However, the tunneling current $\langle J^{\mathrm{tun}}\rangle_k$ may in principle be nonvanishing in the ground state: Eq. (10) is indeed the discrete counterpart of the Schrödinger probability current, as discussed in Ref. [30]. We find nevertheless that also $\langle J^{\mathrm{tun}}\rangle_k$ vanishes in the ground state of (1) for any f. In Appendix B, we consider the rotated model of (1) with $\sigma \to \mu$ and $\mu \to \sigma$, and interestingly find that the $\langle J^{\mathrm{tun}}\rangle_k$ shown a critical-like behavior in the ground state, being nonzero for $f \lesssim f_c$.

IV. CONNECTING CURRENTS TO COLLECTIVE INFORMATION THEORETIC QUANTITIES

The connection between the location, in parameter space, of the quantum critical point of the CCM and that of the optimal particle currents is suggestive of a potential role of collective quantum phenomena in the establishment of the nonequilibrium features of the system. In this section, we explore such suggestion further by making use of a toolbox of information theoretic figures of merit that have been used, in the past, to explore the interplay between quantum critical phenomena and nonclassicality [46,63,64]. In doing so, we unveil the intrinsically collective nature of the features that have been highlighted in our analysis so far.

Quantitatively, we will consider the von Neumann entropy of a subsystem A of a compound $A \cup B$, which is defined as

$$S_A = -\mathrm{Tr}[\rho_A \ln \rho_A], \tag{12}$$

where $\rho_A = \mathrm{Tr}_B[\rho]$ denotes the partial trace over B. Another relevant measure is the negativity N_A [65], which is able to quantify entanglement and is given by

$$N_A = \sum_{\lambda_n < 0} |\lambda_n|, \tag{13}$$

where $\rho^{T_A} = \sum_n \lambda_n |n\rangle\langle n|$ is the spectral decomposition of the partially transposed state with respect to subsystem A. The total amount of correlations (classical and quantum) shared between the bipartitions A and B can be quantified using on the mutual information

$$I(A:B) = S_A + S_B - S_{A \cup B}, \tag{14}$$

where $S_{A \cup B}$ is the von Neumann entropy of the state of the whole compound. In addition, we shall compute the coherence of the system state using the L_1 norm [66]

$$C(\rho) = \sum_{i \neq j} |\rho_{i,j}|, \tag{15}$$

where $\rho_{i,j}$ are the density matrix entries in the clock-state basis. Finally, we will use the quantifier of multipartite quantum correlations provided by the so-called global quantum discord [46,63]

$$\mathcal{G}(\rho) = \min_{\Pi^k} \left\{ S(\rho || \Pi(\rho)) - \sum_{i=1}^{M} S(\rho_i || \Pi_i(\rho_i)) \right\}, \tag{16}$$

where ρ_i denotes the reduced state of the ith rotor, $\Pi(\rho) = \sum_j \Pi^j \rho \Pi^j$ is a projector operator acting on the global state, and $\Pi_i(\rho_i)$ the corresponding projector acting on the single-rotor states. Following Ref. [63], we choose $\Pi^j = \mathcal{R}|j\rangle\langle j|\mathcal{R}^\dagger$ with $\mathcal{R} = \otimes_{i=1}^{M} R_i(\theta_i)$ a collection of single-particle rotation operators, while the operator acting on the ith rotor reads

$$R_i(\theta_i) = e^{i\boldsymbol{\theta}_i \cdot \boldsymbol{\Lambda}}, \tag{17}$$

where $\boldsymbol{\theta}_i = (\theta_{i,1}, \theta_{i,2}, \ldots, \theta_{i,n_a})$ is a vector of n_a angles, and $\boldsymbol{\Lambda} = (\Lambda_1, \Lambda_2, \ldots, \Lambda_{n_a})$ is a vector of generators of rotations for the single rotor. We have considered the $n_a = 8$ Gell-Mann 3×3 matrices as generators of rotations. The minimum in Eq. (16) is obtained by varying the set of angles $\{\boldsymbol{\theta}_i\}$, $i = 1, \ldots, M$, through an annealing algorithm.

These instruments are all very informative of the quantum critical features of the ground-state QPT [44,45] in the CCM (cf. Appendix A). Here however we are mainly interested in the NESS properties. In such an open quantum system, critical features become blurred or disappear altogether. This might lead one to naively think that no connection could be established. Yet, the interplay between temperature gradient between sub-lattices, currents, and correlations reveal a rich phenomenology. Figure 5 shows the behavior of these quantities for different parameters. Contrary to the CCM ground state, these quantities show a smooth dependence on f, which suggests that it is not in partition-dependent quantities that a behavior reminiscent of a critical one should be sought. However, it is interesting to observe that both S_A and $I(A:B)$ have an inflexion point in the region where we expect the critical value of f to occur, which indicates a qualitative change in trend taking place around $f \simeq 0.46$. On the other hand, the global quantum discord shows the nonclassical nature of the state of the NESS away from $f = 0, 1$, which correlates with
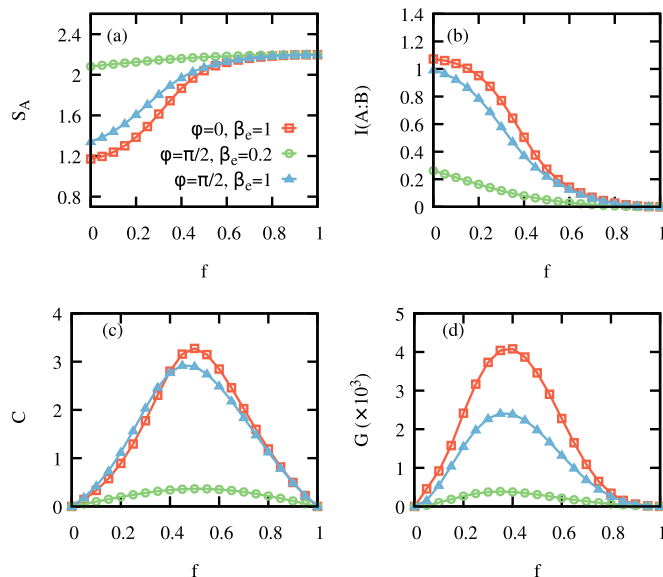
FIG. 5. Information measures of the NESS for $M = 4$ rotors as a function of the control parameter f. (a)–(d) show the von Neumann entropy S_A, mutual information $I(A:B)$, coherence C and global discord, respectively, with A denoting the first half of the chain, namely, rotors 1 and 2. Different points (and colors) correspond to distinct values of the staggered chiral phase, such that $\varphi_k = (-1)^k \varphi$, and local temperature β_e, while $g = 0.2$ and $\beta_o = 1.1$. See main text for further details.

the amount of coherence C. However, while the coherence for the chiral model is maximum at $f \simeq 0.46$, the global discord peaks at a slightly smaller value of f, likely as a result of finite-size effects that are manifested differently in C and the global discord, the latter being, in general, a non linear function of the elements of the density matrix. This should be compared with Figs. 2(a) and 2(b) and Figs. 3(a) and 3(b), which show a similar behavior for the tunneling and thermal currents. This suggests that the degree of nonclassicality of the state of the system, as characterized by the coherence and the global discord, might play an important role for the out-of-equilibrium CCM to work as a thermal machine, thus converting heat currents into mechanical currents.

Note however, that although ρ_{SS} contains coherence for $f \neq 0, 1$, its maximum value is significantly smaller than in the ground-state where $C \propto N_s^M$ for $f > f_c$ [cf. Fig. 8(d)]. Similar behavior is observed for other choices of φ, also for $\varphi = q\pi/N_s$ with $q \in \mathbb{Z}$. In addition, all these quantities inherit the periodicity $2\pi/N_s$ in the phase φ. Finally, we stress that $N_A = 0 \,\forall f, \varphi$, in contrast to the ground-state negativity (cf. Appendix A).

The observed behavior of the mutual information correlates with that of the total current $\langle J^{\mathrm{th}} + J^{\mathrm{tun}}\rangle_T \approx \langle J^{\mathrm{th}}\rangle_T$ [cf. Figs. 3(b) and 5(b)]. Building on this observation, we investigate the thermal susceptibility of the total current $\langle \Delta J^{\mathrm{th}}\rangle_T / \Delta T$ with that of the mutual information, $\Delta I(A : B)/\Delta T$ when $\Delta T \to 0$, where $\langle \Delta J^{\mathrm{th}}\rangle_T \equiv \langle J^{\mathrm{th}}(\Delta T)\rangle_T - \langle J^{\mathrm{th}}(\Delta T = 0)\rangle_T$ denotes the increment in the total current between $0 < |\Delta T| \ll 1$ and $\Delta T = 0$ (equal temperatures for both sub-lattices), and equivalently for the mutual information. Note that since $\langle J^{\mathrm{th}}(\Delta T = 0)\rangle_T = 0$, it follows
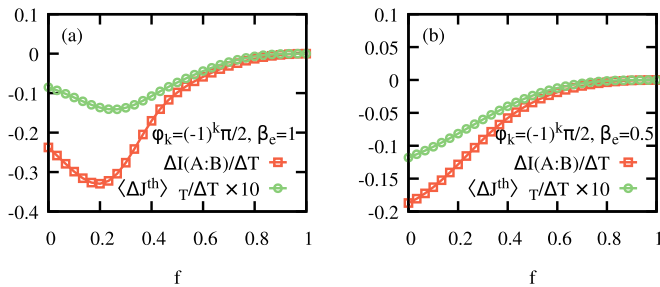
FIG. 6. Mutual information and current susceptibilities, $\Delta I(A : B)/\Delta T$, $\langle \Delta J^{\text{th}} \rangle_T / \Delta T$ as a function of the control parameter for $M = 4$ rotors and $\varphi_k = (-1)^k \pi/2$. (a) and (b) correspond to $\beta_e = 1$ and $\beta_e = 0.5$, respectively, such that $\beta_o = 1/(T_e + \Delta T)$ with $\Delta T = 10^{-3}$, and $g = 0.2$. The current susceptibility is multiplied by a factor 10 for a better representation. Both quantities feature a qualitatively similar behavior.

$\langle \Delta J^{\text{th}} \rangle_T / \Delta T = \langle J^{\text{th}}(\Delta T) \rangle_T / \Delta T$. In order to illustrate this susceptibility, we fix $\beta_e = 1/T_e$ and change $\beta_o = 1/(T_e + \Delta T)$ for $|\Delta T| \ll 1$. In Fig. 6, we show two examples of the mutual information and current susceptibility for $\Delta T = 0.001$ and different T_e, for a fixed $\varphi_k = (-1)^k \pi/2$. Both susceptibilities feature a qualitative similar behavior, as well as for other choices of the parameters. We stress however that for different choices of φ (or β_o) one may revert their relative sign. In addition, one should note that the total current vanishes for $\varphi = q\pi/N_s$ with $q \in \mathbb{Z}$, while the mutual information does not.

V. CONCLUSIONS

We have addressed the link between the emergence of NESS currents in a chiral few-body interacting-clock model and critical features of the corresponding model at the thermodynamic limit: The response of the system, in terms of currents, is maximum at the working point where a QPT is predicted to occur. This is also well captured by the behavior of genuinely multipartite information theoretic quantities, such as global quantum discord, and provides strong numerical evidences of the possible role that collective quantum phenomena play in the nonequilibrium response of this interesting interacting model. Such link will be explored further in future works through the investigation of possible effects in work-extraction games aimed at achieving ergotropic performance from the thermal-to-mechanical current-conversion process that we have addressed here.

Furthermore, the investigation of the dynamical properties of the ground state of the model (1) and its variations is an interesting open question. In particular we find that tunneling currents can arise in a rotated version of (1) with a finite number of rotors. Whether such currents persist in the thermodynamic limit and exhibit a critical behavior are questions worthy of future studies.

ACKNOWLEDGMENTS

APPENDIX A: CRITICAL GROUND STATE FEATURES IN THE CHIRAL CLOCK MODEL

As already noted, the CCM exhibits a $\mathbb{Z}_{N_s}$ symmetry. In order to exploit this symmetry, it is handy to remap the Hamiltonian as $\sigma \to \mu$ and $\mu \to \sigma$ (as in Ref. [50]), so that the operator

$$\mathcal{U} = \prod_{k=1}^{M} \mu_k^\dagger, \tag{A1}$$

allows us to split the Hilbert space in N_s subspaces. The ground state is contained in the subspace with eigenvalue 1. In the case of $N_s = 3$, the operator reads as $\mathcal{U} = \Pi_0 \Pi_0^\dagger + \upsilon \Pi_1 \Pi_1^\dagger + \upsilon^2 \Pi_2 \Pi_2^\dagger$, where Π_n denotes the projector on the corresponding subspace. One can use this symmetry to reduce the dimension of the Hilbert space. In particular,

$$H_{\text{ccm}}^0 = \Pi_0 H_{\text{ccm}} \Pi_0^\dagger \tag{A2}$$
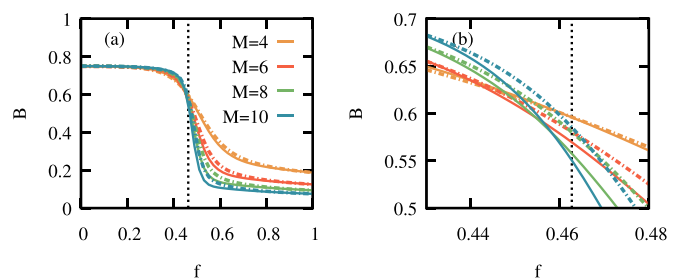
FIG. 7. (a) Binder cumulant B for the ground state of the CCM with $N_s = 3$ for different system sizes (from $M = 4$ to 10 rotors) as function of f and with $\varphi_k = \pi/8$ (solid lines) and staggered chiral phase $\varphi_k = (-1)^k \pi/8$ (dashed lines). The vertical dotted line indicates the critical value f_c where the QPT takes place, reported in Ref. [50]. (b) shows a zoom close to the region where Binder cumulants intersect (close to f_c). For homogeneous chiral phase, the crossing approaches the reported value f_c. The intersections in B for staggered chiral phases suggests that location of f_c is shifted to a slightly larger value.
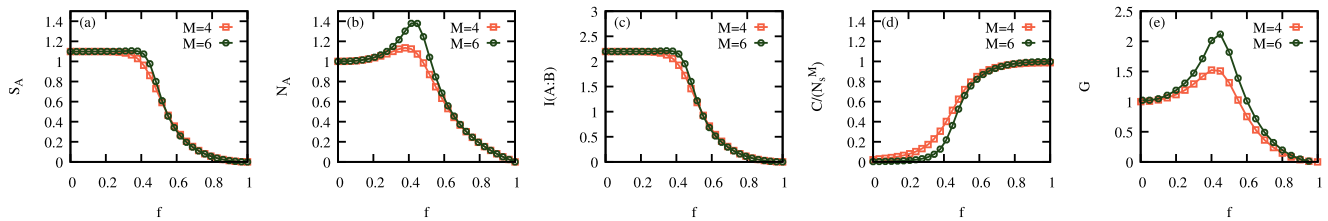
FIG. 8. Quantum information measures of the ground state of the CCM with periodic boundary conditions and staggered chiral phase $\varphi_k = (-1)^k \pi/2$ for $M = 4$ and 6 rotors, which unveil the QPT taking place in the system. From left to right, von Neumann entropy S_A, negativity N_A, mutual information $I(A:B)$, coherence C (rescaled over the total Hilbert space dimension N_s^M), and global discord $\mathcal{G}$, respectively. The system is split in half, so the partition A includes the first $M/2$ rotors, namely, rotors 1 and 2 for $M = 4$ and 1, 2 3 for $M = 6$.

contains the ground state $\forall f$ with a well defined symmetry. For $f < f_c$, the ground state becomes N_s-fold degenerate. In Ref. [50], the ground-state energy critical exponents of the H_{ccm} were investigated. For completeness, here we just provide a brief summary of the critical features of such a model. In particular, note that the ground-state order parameter $m = \frac{1}{M} \sum_{k=1}^{M} (\mu_k + \mu_k^\dagger)$ within the Π_0 subspace is given by

$$\langle \varphi(f) | m | \varphi(f) \rangle \equiv 0 \quad \forall f, \tag{A3}$$

where $|\varphi(f)\rangle$ denotes the ground state of H_{ccm}^0. As customary in symmetry-breaking phase transitions, one needs to resort to m^2 and m^4, which clearly reveal the symmetry-broken phase for $f < f_c$ (and thus the QPT). Moreover, the location of the QPT can be witnessed by looking at the energy gap Δ or Binder cumulant B [67]. The energy gap between the ground and first excited state closes at f_c following the universal scaling law [43]

$$\Delta \sim |f - f_c|^{z\nu}. \tag{A4}$$

where $z\nu$ are critical exponents of the QPT. The Binder cumulant is defined as [67]

$$B = \frac{1}{2} \left(3 - \frac{\langle m^4 \rangle}{\langle m^2 \rangle^2} \right) \tag{A5}$$

where $\langle m^4 \rangle$ and $\langle m^2 \rangle$ are evaluated over the ground state, i.e., $\langle \varphi(f) | m^2 | \varphi(f) \rangle$ and $\langle \varphi(f) | m^4 | \varphi(f) \rangle$. This quantity has been proven very useful to locate the critical point f_c (see for example Refs. [68,69]). Applying finite-size scaling arguments, B is expected to become size independent at f_c. Hence, the QPT takes place at the value of f at which the Binder cumulant B for different system sizes M intersect, although finite-size corrections still yield small deviations to the size-independent intersections. In Fig. 7 we show the resulting Binder cumulant B for the ground state of the CCM for $N_s = 3$ for the case of a staggered and homogeneous chiral phase $\varphi_k = (-1)^k \pi/8$ and $\varphi_k = \pi/8$, respectively. The location of the QPT, i.e. f_c, for the homogeneous chiral phase is consistent with the reported value in Ref. [50], $f_c = 0.46267$ which is indicated by a dotted vertical line, while f_c appears to be shifted to a slightly larger value for a staggered chiral phase. The signatures of the QPT are already evident even for the considered system sizes $M \lesssim 10$.

In addition, in Fig. 8 we show the quantum information measures on the CCM ground-state as a function of the control parameter f, namely, von Neumann entropy S_A, negativity N_A,

coherence C, mutual information $I(A:B)$ and global quantum discord $\mathcal{G}$. The system is split in half, so that A refers to the first two rotors for $M = 4$. All the quantities indicate a QPT taking place at $f \approx 0.46$ [50]. Compare these ground-state results with those discussed in the main text for the NESS. It is worth noting that the nonchiral model $\varphi_k = 0$ has a critical field $f_c = 1/2$ [50], thus the chirality lowers the value of the field required to achieve the disordered phase, as one would expect.

APPENDIX B: TUNNELING CURRENT IN A ROTATED CCM MODEL

As commented in the main text, while the ground-state properties of the CCM model remain unaltered upon the rotation $\sigma \to \mu$ and $\mu \to \sigma$, the tunneling current becomes remarkably different. Note that the definition of the tunneling current $J^{tun}(j \to j')$ given in Eq. (10) is independent of the specific choice of the Hamiltonian. In particular, for

$$\tilde{H}_{ccm} = -f \sum_{k=1}^{M} (\mu_k + \mu_k^+) - (1-f) \sum_{k=1}^{M} (\sigma_k \sigma_{k+1}^\dagger e^{i\varphi_k} + \text{H.c.}), \tag{B1}$$

with staggered chiral phases $\varphi_k = (-1)^k \varphi$, the tunneling current in its ground state is non zero. Moreover, the behavior of J^{tun} resembles that of a critical quantity across a phase transition. The resulting tunneling current for a parity-preserving ground state is plotted in Fig. 9 for M from 4 to 12 rotors, which indicate a sharp transition around the QPT.
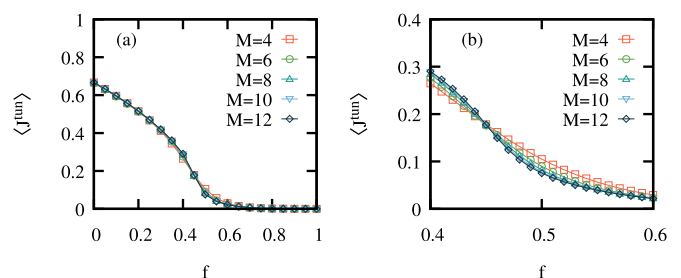
FIG. 9. (a) Tunneling current for the odd rotors $\langle J^{tun} \rangle$ in the ground state of the CCM $\tilde{H}_{ccm}$, given in Eq. (B1), with $\varphi_k = (-1)^k \pi/2$ and as a function of f. The tunneling current for even rotors is reversed in sign, i.e., $-\langle J^{tun} \rangle$. (b) shows a zoom closer to the transition point to signal the sharper behavior of $\langle J^{tun} \rangle$ as M increases.

[1] T. B. Batalhão, A. M. Souza, L. Mazzola, R. Auccaise, R. S. Sarthour, I. S. Oliveira, J. Goold, G. De Chiara, M. Paternostro, and R. M. Serra, Experimental Reconstruction of Work Distribution and Study of Fluctuation Relations in a Closed Quantum System, Phys. Rev. Lett. **113**, 140601 (2014).

[2] F. Brandão, M. Horodecki, N. Ng, J. Oppenheim, and S. Wehner, The second laws of quantum thermodynamics, Proc. Natl. Acad. Sci. USA **112**, 3275 (2015).

[3] A. M. Alhambra, L. Masanes, J. Oppenheim, and C. Perry, Fluctuating Work: From Quantum Thermodynamical Identities to a Second Law Equality, Phys. Rev. X **6**, 041017 (2016).

[4] M. Brunelli, L. Fusco, R. Landig, W. Wieczorek, J. Hoelscher-Obermaier, G. Landi, F. L. Semião, A. Ferraro, N. Kiesel, T. Donner, G. De Chiara, and M. Paternostro, Experimental Determination of Irreversible Entropy Production in out-of-Equilibrium Mesoscopic Quantum Systems, Phys. Rev. Lett. **121**, 160604 (2018).

[5] G. T. Landi and M. Paternostro, Irreversible entropy production, from quantum to classical, Rev. Mod. Phys. **93**, 035008 (2021).

[6] R. Kosloff, A quantum mechanical open system as a model of a heat engine, J. Chem. Phys. **80**, 1625 (1984).

[7] N. Linden, S. Popescu, and P. Skrzypczyk, How Small Can Thermal Machines Be? The Smallest Possible Refrigerator, Phys. Rev. Lett. **105**, 130401 (2010).

[8] O. Abah, J. Roßnagel, G. Jacob, S. Deffner, F. Schmidt-Kaler, K. Singer, and E. Lutz, Single-Ion Heat Engine at Maximum Power, Phys. Rev. Lett. **109**, 203006 (2012).

[9] J. Roßnagel, O. Abah, F. Schmidt-Kaler, K. Singer, and E. Lutz, Nanoscale Heat Engine Beyond the Carnot Limit, Phys. Rev. Lett. **112**, 030602 (2014).

[10] J. Roßnagel, S. T. Dawkins, K. N. Tolazzi, O. Abah, E. Lutz, F. Schmidt-Kaler, and K. Singer, A single-atom heat engine, Science **352**, 325 (2016).

[11] J. P. S. Peterson, T. B. Batalhão, M. Herrera, A. M. Souza, R. S. Sarthour, I. S. Oliveira, and R. M. Serra, Experimental Characterization of a Spin Quantum Heat Engine, Phys. Rev. Lett. **123**, 240601 (2019).

[12] D. von Lindenfels, O. Gräb, C. T. Schmiegelow, V. Kaushal, J. Schulz, M. T. Mitchison, J. Goold, F. Schmidt-Kaler, and U. G. Poschinger, Spin Heat Engine Coupled to a Harmonic-Oscillator Flywheel, Phys. Rev. Lett. **123**, 080602 (2019).

[13] R. Dorner, J. Goold, C. Cormick, M. Paternostro, and V. Vedral, Emergent Thermodynamics in a Quenched Quantum Many-Body System, Phys. Rev. Lett. **109**, 160601 (2012).

[14] G. Watanabe, B. P. Venkatesh, P. Talkner, M.-J. Hwang, and A. del Campo, Quantum Statistical Enhancement of the Collective Performance of Multiple Bosonic Engines, Phys. Rev. Lett. **124**, 210603 (2020).

[15] A. Hartmann, V. Mukherjee, W. Niedenzu, and W. Lechner, Many-body quantum heat engines with shortcuts to adiabaticity, Phys. Rev. Res. **2**, 023145 (2020).

[16] Z. Fei, N. Freitas, V. Cavina, H. T. Quan, and M. Esposito, Work Statistics across a Quantum Phase Transition, Phys. Rev. Lett. **124**, 170603 (2020).

[17] T. Fogarty and T. Busch, A many-body heat engine at criticality, Quantum Sci. Technol. **6**, 015003 (2021).

[18] R. B. S, V. Mukherjee, U. Divakaran, and A. del Campo, Universal finite-time thermodynamics of many-body quantum machines from Kibble-Zurek scaling, Phys. Rev. Res. **2**, 043247 (2020).

[19] R. Filliger and P. Reimann, Brownian Gyrator: A Minimal Heat Engine on the Nanoscale, Phys. Rev. Lett. **99**, 230602 (2007).

[20] V. Dotsenko, A. Maciołek, O. Vasilyev, and G. Oshanin, Two-temperature langevin dynamics in a parabolic potential, Phys. Rev. E **87**, 062130 (2013).

[21] A. Argun, J. Soni, L. Dabelow, S. Bo, G. Pesce, R. Eichhorn, and G. Volpe, Experimental realization of a minimal microscopic heat engine, Phys. Rev. E **96**, 052106 (2017).

[22] V. Mancois, B. Marcos, P. Viot, and D. Wilkowski, Two-temperature Brownian dynamics of a particle in a confining potential, Phys. Rev. E **97**, 052121 (2018).

[23] H. C. Fogedby and A. Imparato, A minimal model of an autonomous thermal motor, Europhys. Lett. **119**, 50007 (2017).

[24] A. Imparato, Out-of-equilibrium Frenkel–Kontorova model, J. Stat. Mech.: Theory Exp. (2021) 013214.

[25] A. Mari, A. Farace, and V. Giovannetti, Quantum optomechanical piston engines powered by heat, J. Phys. B: At. Mol. Opt. Phys. **48**, 175501 (2015).

[26] A. Roulet, S. Nimmrichter, J. M. Arrazola, S. Seah, and V. Scarani, Autonomous rotor heat engine, Phys. Rev. E **95**, 062131 (2017).

[27] S. Seah, S. Nimmrichter, and V. Scarani, Work production of quantum rotor engines, New J. Phys. **20**, 043045 (2018).

[28] H. C. Fogedby and A. Imparato, Autonomous quantum rotator, Europhys. Lett. **122**, 10006 (2018).

[29] A. Roulet, S. Nimmrichter, and J. M. Taylor, An autonomous single-piston engine with a quantum rotor, Quantum Sci. Technol. **3**, 035008 (2018).

[30] K. V. Hovhannisyan and A. Imparato, Quantum current in dissipative systems, New J. Phys. **21**, 052001 (2019).

[31] M. Drewsen and A. Imparato, Quantum duets working as autonomous thermal motors, Phys. Rev. E **100**, 042138 (2019).

[32] P. P. Hofer, M. Perarnau-Llobet, J. B. Brask, R. Silva, M. Huber, and N. Brunner, Autonomous quantum refrigerator in a circuit qed architecture based on a Josephson junction, Phys. Rev. B **94**, 235420 (2016).

[33] A. Hewgill, J. O. González, J. P. Palao, D. Alonso, A. Ferraro, and G. De Chiara, Three-qubit refrigerator with two-body interactions, Phys. Rev. E **101**, 012109 (2020).

[34] A. Hewgill, G. De Chiara, and A. Imparato, Quantum thermodynamically consistent local master equations, Phys. Rev. Res. **3**, 013165 (2021).

[35] N. Golubeva and A. Imparato, Efficiency at Maximum Power of Interacting Molecular Machines, Phys. Rev. Lett. **109**, 190602 (2012).

[36] N. Golubeva and A. Imparato, Maximum power operation of interacting molecular motors, Phys. Rev. E **88**, 012114 (2013).

[37] N. Golubeva and A. Imparato, Efficiency at maximum power of motor traffic on networks, Phys. Rev. E **89**, 062118 (2014).

[38] A. Imparato, Stochastic thermodynamics in many-particle systems, New J. Phys. **17**, 125004 (2015).

[39] T. Herpich, J. Thingna, and M. Esposito, Collective Power: Minimal Model for Thermodynamics of Nonequilibrium Phase Transitions, Phys. Rev. X **8**, 031056 (2018).

[40] T. Herpich and M. Esposito, Universality in driven Potts models, Phys. Rev. E **99**, 022135 (2019).

[41] M. Suñé and A. Imparato, Out-of-Equilibrium Clock Model at the Verge of Criticality, Phys. Rev. Lett. **123**, 070601 (2019).

[42] K. Huang, *Statistical Mechanics* (John Wiley & Sons, Inc., New York, 1987).

[43] S. Sachdev, *Quantum Phase Transitions*, 2nd ed. (Cambridge University Press, Cambridge, UK, 2011).

[44] T. J. Osborne and M. A. Nielsen, Entanglement in a simple quantum phase transition, Phys. Rev. A **66**, 032110 (2002).

[45] G. Vidal, J. I. Latorre, E. Rico, and A. Kitaev, Entanglement in Quantum Critical Phenomena, Phys. Rev. Lett. **90**, 227902 (2003).

[46] G. De Chiara and A. Sanpera, Genuine quantum correlations in quantum many-body systems: a review of recent progress, Rep. Prog. Phys. **81**, 074002 (2018).

[47] P. Fendley, Parafermionic edge zero modes in Zn-invariant spin chains, J. Stat. Mech. (2012) P11020.

[48] G. Ortiz, E. Cobanera, and Z. Nussinov, Dualities and the phase diagram of the p-clock model, Nucl. Phys. B **854**, 780 (2012).

[49] S. Whitsitt, R. Samajdar, and S. Sachdev, Quantum field theory for the chiral clock transition in one spatial dimension, Phys. Rev. B **98**, 205118 (2018).

[50] R. Samajdar, S. Choi, H. Pichler, M. D. Lukin, and S. Sachdev, Numerical study of the chiral $\mathbb{z}_3$ quantum phase transition in one spatial dimension, Phys. Rev. A **98**, 023614 (2018).

[51] N. Nishad, M. Santhosh, and G. J. Sreejith, Postquench entropy growth in a chiral clock model, Phys. Rev. B **103**, 195141 (2021).

[52] N. Nishad and G. J. Sreejith, Energy transport in Z3 chiral clock model, New J. Phys. **24**, 013035 (2022).

[53] C. M. Lapilli, P. Pfeifer, and C. Wexler, Universality Away from Critical Points in Two-Dimensional Phase Transitions, Phys. Rev. Lett. **96**, 140603 (2006).

[54] H. Bernien, S. Schwartz, A. Keesling, H. Levine, A. Omran, H. Pichler, S. Choi, A. S. Zibrov, M. Endres, M. Greiner, V. Vuletić, and M. D. Lukin, Probing many-body dynamics on a 51-atom quantum simulator, Nature (London) **551**, 579 (2017).

[55] J. M. Horowitz and J. M. R. Parrondo, Entropy production along nonequilibrium quantum jump trajectories, New J. Phys. **15**, 085028 (2013).

[56] H.-P. Breuer and F. Petruccione, *The Theory of Open Quantum Systems* (Oxford University Press, Oxford, UK, 2002).

[57] A. Levy and R. Kosloff, The local approach to quantum transport may violate the second law of thermodynamics, Europhys. Lett. **107**, 20004 (2014).

[58] J. T. Stockburger and T. Motz, Thermodynamic deficiencies of some simple lindblad operators, Fortschr. Phys. **65**, 1600067 (2017).

[59] F. Barra, The thermodynamic cost of driving quantum systems by their boundaries, Sci. Rep. **5**, 14873 (2015).

[60] P. Strasberg, G. Schaller, T. Brandes, and M. Esposito, Quantum and Information Thermodynamics: A Unifying Framework Based on Repeated Interactions, Phys. Rev. X **7**, 021003 (2017).

[61] G. De Chiara, G. Landi, A. Hewgill, B. Reid, A. Ferraro, A. J. Roncaglia, and M. Antezza, Reconciliation of quantum local master equations with thermodynamics, New J. Phys. **20**, 113024 (2018).

[62] P. Potts, A. Arash Sand Kalaee, and A. Wacker, A thermodynamically consistent Markovian master equation beyond the secular approximation, New J. Phys. **23**, 123013 (2021).

[63] S. Campbell, L. Mazzola, G. D. Chiara, T. J. G. Apollaro, F. Plastina, T. Busch, and M. Paternostro, Global quantum correlations in finite-size spin chains, New J. Phys. **15**, 043033 (2013).

[64] S. Campbell, L. Mazzola, and M. Paternostro, Global quantum correlations in the Ising model, Int. J. Quant. Inf. **09**, 1685 (2011).

[65] G. Vidal and R. F. Werner, Computable measure of entanglement, Phys. Rev. A **65**, 032314 (2002).

[66] T. Baumgratz, M. Cramer, and M. B. Plenio, Quantifying Coherence, Phys. Rev. Lett. **113**, 140401 (2014).

[67] K. Binder, Finite size scaling analysis of ising model block distribution functions, Z. Phys. B **43**, 119 (1981).

[68] M. C. Angelini, G. Parisi, and F. Ricci-Tersenghi, Relations between short-range and long-range Ising models, Phys. Rev. E **89**, 062120 (2014).

[69] R. Puebla, O. Marty, and M. B. Plenio, Quantum Kibble-Zurek physics in long-range transverse-field Ising models, Phys. Rev. A **100**, 032115 (2019).